

# Numerical and Experimental Investigations of Channel Flows in a Disk-Type Drag Pump

Young-Kyu Hwang, Joong-Sik Heo and Wook-Jin Choi

*School of Mechanical Engineering, Sungkyunkwan University, 300 Chunchun-dong, Jangan-ku, Suwon 440-746, S. Korea*

**Abstract.** Pumping performance of a disk-type drag pump is studied numerically and experimentally. Molecular transition and slip flows that arise in a spiral channel on the rotating disk are simulated by using particle and continuum methods. The particle approach employs the direct simulation Monte Carlo (DSMC) method, and the continuum approach solves the Navier-Stokes (N-S) equations. A new DSMC code that can handle noninertial effects existing in the rotating frame of reference is developed. In this DSMC code, particular attention is paid to matching the solutions obtained by the N-S method in the slip flow regime. In the experimental study, the inlet pressures are measured for various outlet pressures of a test pump. Comparison between the experimental data and the numerical results reveals that the DSMC method provides the more accurate solution of the rarefied channel flow for the range of Knudsen number  $Kn > 0.02$  than does the N-S method.

## INTRODUCTION

Molecular drag stages are commonly used in combination with turbomolecular stages, permitting higher discharge pressures and larger throughput capabilities compared to conventional turbomolecular pumps.[1] Many investigations have been done toward developing theories of the rarefied gas flows in channels of a disk-type drag pump (DTDP). Liu and Pang[2] studied the performance of a spiral channel on the disk of a DTDP in free molecular flow by using the matrix-probability method. Shi *et al.*[3,4] theoretically investigated the influence of geometrical parameters of a spiral channel on performance by the test particle Monte Carlo method. According to their studies, the pumping performance is strongly dependent on the rotational speed and geometrical parameters. Although knowledge of the performance in the molecular transition regime is very important in applications, the previous studies[2-4] were inherently based on the free molecular flow assumptions.

Recently, Cheng *et al.*[5] studied the continuum and slip flows in a DTDP by using the Navier-Stokes (N-S) equations with no-slip conditions and energy equation. Finite difference approximations were employed to discretize the transport equations on a body-fitted grid system. Their numerical results were in good agreement with the experimental data in the continuum flow. But it was found that the N-S equations were not valid to predict the performance of a DTDP in the molecular transition regime.

Heo and Hwang[6] numerically studied the molecular transition and slip flows by using both the direct simulation Monte Carlo (DSMC) method and the N-S equations with slip boundary conditions (SBC). For a helical-type drag pump, they found that the numerical results obtained by both methods agree well with the experimental data for the Knudsen number  $Kn \leq 0.01$ . But the results from the DSMC method were only reasonable in the molecular transition regime for  $Kn \geq 0.01$ . The present paper is an extended report of the previous study.[6]

In this study, the pumping performance of a DTDP is numerically and experimentally analyzed. First, the velocity and density fields are predicted by using the DSMC method. Second, our experimental results are presented in the pressure range of 0.1 ~ 4 Torr and are compared with numerical ones obtained by the DSMC and N-S methods. The formulation of second-order SBC is utilized in the N-S method. A particular attention is paid to matching the DSMC method with the solutions obtained by the N-S method in the slip flow regime.

## Report Documentation Page

<b>Report Date</b> 09JUL2000	<b>Report Type</b> N/A	<b>Dates Covered (from... to)</b> -
<b>Title and Subtitle</b> Numerical and Experimental Investigations of Channel Flows in a Disk-Type Drag Pump	<b>Contract Number</b>	
	<b>Grant Number</b>	
	<b>Program Element Number</b>	
<b>Author(s)</b>	<b>Project Number</b>	
	<b>Task Number</b>	
	<b>Work Unit Number</b>	
<b>Performing Organization Name(s) and Address(es)</b> School of Mechanical Engineering, Sungkyunkwan University, 300 Chunchun-dong, Jangan-ku, Suwon 440-746, S. Korea	<b>Performing Organization Report Number</b>	
<b>Sponsoring/Monitoring Agency Name(s) and Address(es)</b> AOARD Unit 45002 APO AP 96337-5002	<b>Sponsor/Monitor's Acronym(s)</b>	
	<b>Sponsor/Monitor's Report Number(s)</b>	
<b>Distribution/Availability Statement</b> Approved for public release, distribution unlimited		
<b>Supplementary Notes</b> Papers from Rarefied Gas Dynamics (RGD) 22nd International Symposium held in Sydney, Australia on 9-14 July 2000. See also ADM001341 for whole conference on cd-rom., The original document contains color images.		
<b>Abstract</b>		
<b>Subject Terms</b>		
<b>Report Classification</b> unclassified	<b>Classification of this page</b> unclassified	
<b>Classification of Abstract</b> unclassified	<b>Limitation of Abstract</b> UU	
<b>Number of Pages</b> 8		

## NUMERICAL METHODS

Pumping channels are cut on a stationary disk (Type-I) or a rotating disk (Type-II), as shown in Fig. 1. The positive rotational speed (+rps) represents the outward pumping direction, whereas the negative rotational speed (-rps) represents the inward pumping direction. Geometrical parameters of a spiral channel are shown in Fig. 2(a), where  $R_1$  and  $R_2$  are the inner and outer radius of the disk, respectively. Pumping channels are the Archimedes' spiral. The Knudsen number is defined as  $Kn = \lambda/d$ , where  $\lambda$  and  $d$  are the mean free path and the channel depth, respectively. The geometrical dimensions of channels are given in Table 1.

The flow occurring in the pumping channel develops from the molecular transition to slip flow traveling downstream. As in the previous study[6], two different numerical methods are used. The first one is the continuum approach, in which the N-S equations with SBC are solved. The second one is the molecular approach, in which the DSMC method[7] is employed to simulate interactive motions of molecules.

### *DSMC simulations*

A 3D body-fitted grid system is used, as shown in Fig. 2(b). More grid points are placed near the outlet region of the channel to handle large pressure gradients. A large number of molecules is uniformly distributed in the computational domain, and the initial velocities of molecules are evaluated from the Maxwellian distribution function. The null-collision technique of Koura[8] is adopted to determine the number of collision pairs selected within a cell during  $\Delta t$ .

In the case of the Type-II channels, the main difficulty in modeling a 3D flow comes from the rotating frame of reference. In particular, trajectories of particles are not straight lines in the rotating frame. Thus, trajectories are calculated by integrating a system of differential equations, including the Coriolis and centrifugal forces. The fourth-order Runge-Kutta algorithm is used to integrate the following equation:

$$a_r = -\omega \times (\omega \times r_{mol}) - 2\omega \times V_{mol}, \quad (1)$$

in which  $a_r$  is the relative acceleration,  $r_{mol}$  and  $V_{mol}$  is the trajectory and the relative velocity of molecules, and  $\omega$  is the angular velocity.

### *N-S simulations*

In the molecular transition regime, the failure of the N-S solutions is stemmed from the continuum assumption of the N-S equations, which can be derived from the Boltzmann equation based on the Chapman-Enskog expansion of the velocity distribution function  $f$ . Naturally, the N-S equations break down in the molecular transition regime.

Therefore the conventional no-slip boundary conditions are necessary to reformulate.

In the slip flow regime, it has generally been recognized that the layer of gas adjacent to the wall is no longer at rest but has a finite slip velocity. Thus the continuum assumption is not valid near the wall. Sawada[9] showed that the N-S equations can be solved numerically for a helical-type drag pump in the slip flow regime if the boundary conditions are modified to include a slip velocity at the wall. The slip velocity on the wall surfaces is given by:

$$u_s = u_w + \frac{2-\sigma}{\sigma} Kn \left( \frac{\partial u}{\partial n} \right)_w, \quad (2)$$

where  $\sigma$  is the accommodation coefficient,  $u_s$  and  $u_w$  refer to the slip velocity and the wall velocity, respectively. In the above,  $n$  is the non-dimensional coordinate perpendicular to the channel wall that is normalized by the channel depth  $d$ , and subscript  $w$  indicates that the variable is evaluated at the wall.

In the present study, the formulation of second-order SBC is utilized in the N-S method. For the second-order modification of Eq. (2), the following slip velocity can be derived in the case of  $\sigma = 1$ :

$$u_s = u_w + Kn \left( \frac{\partial u}{\partial n} \right)_w + \frac{Kn^2}{2} \left( \frac{\partial^2 u}{\partial n^2} \right)_w. \quad (3)$$

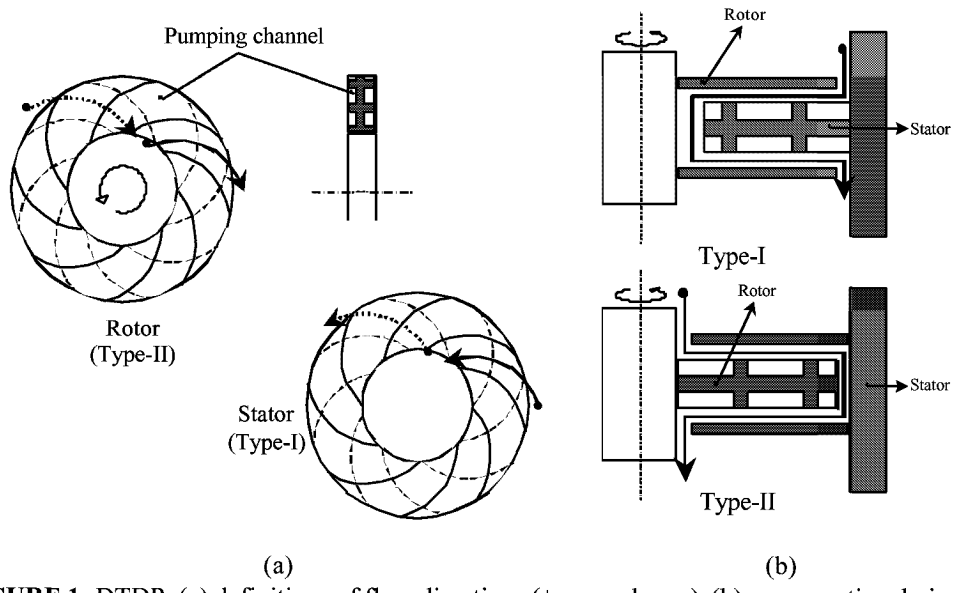


FIGURE 1. DTDP: (a) definitions of flow directions (+rps and -rps); (b) cross-sectional view.

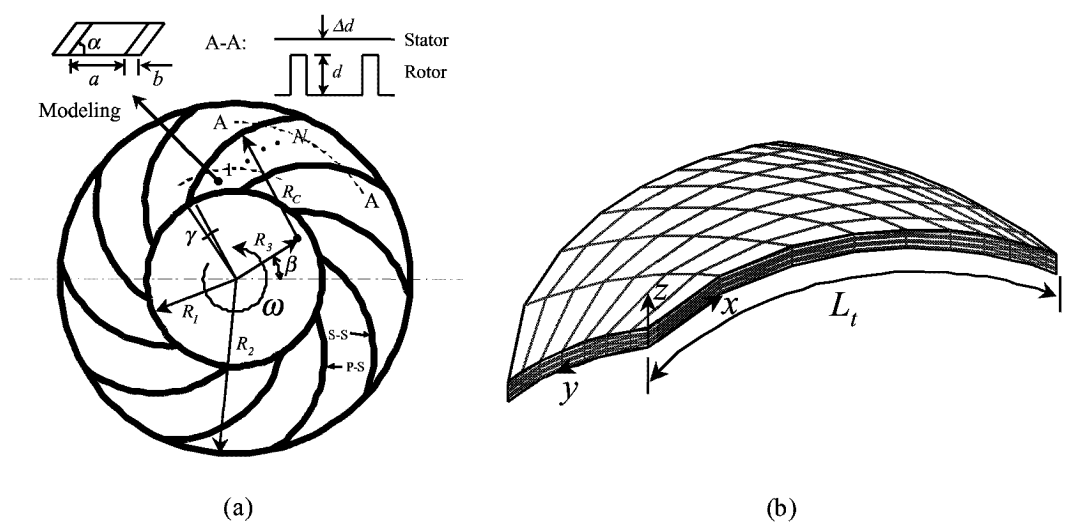


FIGURE 2. DTDP: (a) geometrical parameters; (b) numerical grid system.

TABLE 1. Geometrical dimensions of spiral rotors

Rotational speed	rps	400	
Inner diameter	$R_1$	43 mm	
Outer diameter	$R_2$	86 mm	
Clearance	$\Delta d$	0.5 mm	
Channel depth	$d$	5 mm	
angle	$\beta$	36°	
Angle of blade thickness	$\gamma$	8°	
Radius	$R_3$	A	B
		39 mm	32 mm
Radius	$R_c$	A	B
		56 mm	56 mm

In the N-S simulations, the spiral channel is divided into  $N$  different short channels (see Fig. 2(a)), and each short channel may be regarded as a helical channel.[9] The outlet pressure  $P_2$  of the first short channel can be calculated, and then  $P_2$  is substituted for the inlet pressure of the next channel. Finally, the outlet pressure of the last channel can be obtained in this way. The accuracy of the calculated results is proportional to the number of short channels, and the converged solution is obtained for  $N \geq 10$ .

## EXPERIMENTAL APPARATUS

Experiments on the pumping characteristics of a DTDP are carried out by using the test pump to verify the present numerical results. The inner and outer radius of the disk are 43.0 mm and 86.0 mm, respectively. It has ten grooves, with channel depth of 5 mm.

A schematic diagram of the experimental apparatus is shown in Fig. 3. This apparatus mainly consists of two parts: the test pump, and instruments that facilitate pressure measurements and flow supply into the test pump. The test pump is connected to a two-stage oil rotary pump (970 l/min). The pressure in the high-vacuum side is measured with a Pirani ( $7.6 \times 10^{-4} \sim 7.6$  Torr) and Penning ( $7.6 \times 10^{-8} \sim 7.6 \times 10^{-3}$  Torr) gauge, and the pressure in the fore-vacuum side is measured with a Pirani gauge. Experiments are performed by varying the outlet pressure  $P_2$  in the range of  $0.1 \text{ Torr} \leq P_2 \leq 4 \text{ Torr}$ . The rotational speed of the rotor is 24,000rpm and is controlled by a frequency converter. Test gas ( $N_2$ ) is supplied through a mass flow controller from a regulated high-pressure cylinder. The motor casing is cooled by water at  $22 \pm 3^\circ$  during operation.

A cross-section of a DTDP is illustrated in Fig. 4. The test pump consists of a plane disk (without grooves), grooved rotor (Type-II, +rps) and stator (Type-I, -rps). Dimensions and shape of the spiral channel for rotor and stator are all the same. The pressure is measured at the inlet side (①), the rotor outlet (②), the stator outlet (③), and the discharge side (④), respectively.

## RESULTS AND DISCUSSION

The DSMC simulations are carried out for the inlet pressure  $P_1 = 0.076$  Torr. Computed results are only concerned with the A-type blade (see TABLE 1), and these results are shown in Figs. 5-8.

The normalized pressure distribution  $P/P_1$  along the pumping channel are presented in Fig. 5, where P-S denotes the pressure surface, and S-S the suction surface; see Fig. 2(a). The pressure increases with flow along the channel. The leakage flow from the adjacent pumping channel occurs due to the pressure difference between P-S and S-S.

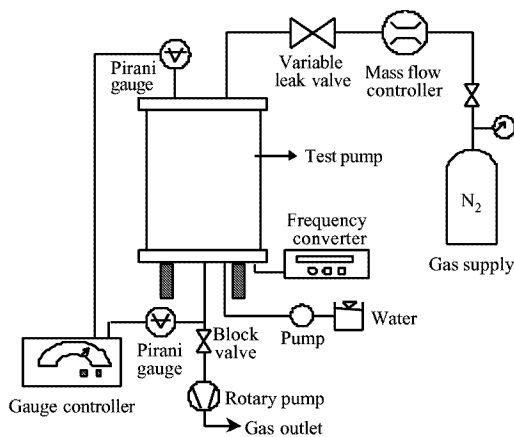


FIGURE 3. Experimental apparatus.

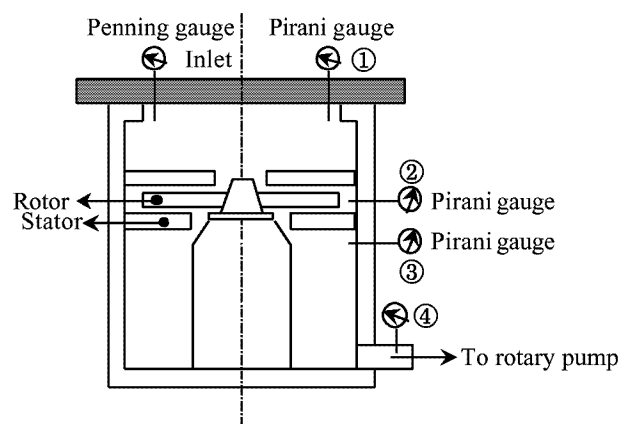
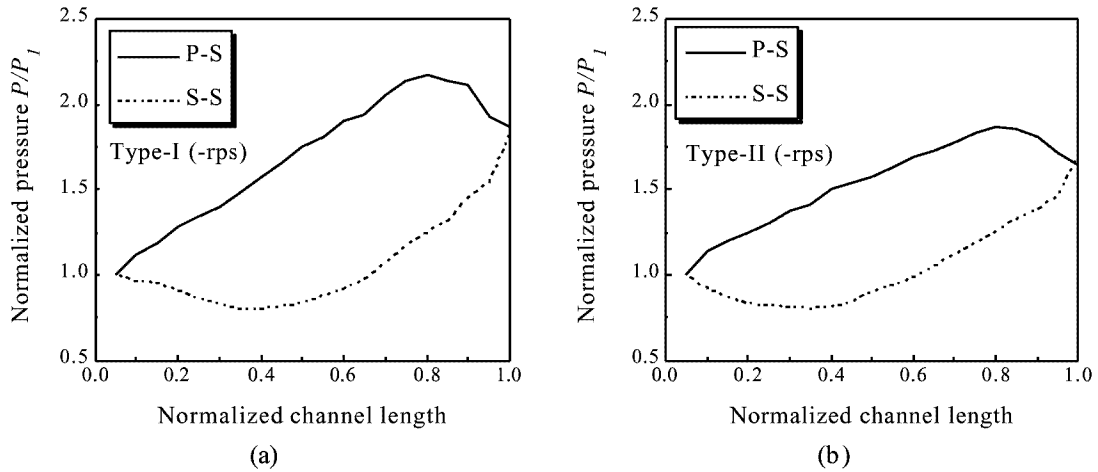
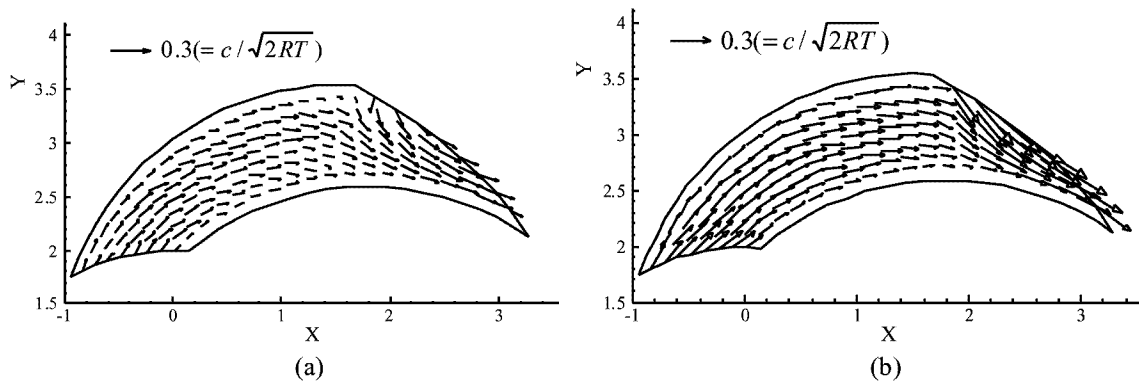


FIGURE 4. Cross-section of a DTDP.



**FIGURE 5.** Pressure distribution  $P/P_1$  along pumping channel at  $P_1=0.076$  Torr: (a) Type-I; (b) Type-II.



**FIGURE 6.** Velocity vectors at  $P_1=0.076$  Torr and  $P_2=0.152$  Torr: (a) Type-I (+rps); (b) Type-II (+rps).

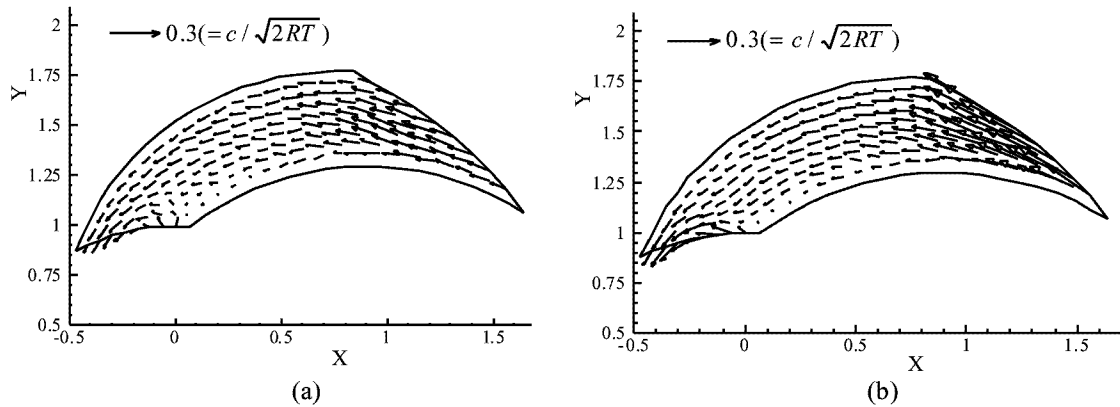


**FIGURE 7.** Velocity vectors at  $P_1=0.076$  Torr and  $P_2=0.152$  Torr: (a) Type-I (-rps); (b) Type-II (-rps).

The velocity vectors, seen in Figs. 6 and 7, are the time-averaged ones during 15,000 time steps. The velocity data are sampled after the flow field reaches steady state and are expressed in dimensionless form  $c/\sqrt{2RT}$ , where  $c$  and  $\sqrt{2RT}$  are the mean molecular velocity and the most probable molecular speed, respectively.

Velocity components of the Type-II channel are larger than those of the Type-I channel because the rotating disk imparts angular momentum directly to the molecules. These figures show a backflow from the outlet to the pumping channel.

The density contours show a large gradient near the outlet, as shown in Fig. 8. The solid and centered lines denote the Type-I and Type-II channels, respectively. In the non-rotating passage (of the Type-I channel), only the curvature effect of the channel wall on the density gradients exists; however, in the rotating passage (of the Type-II channel), Coriolis and centrifugal forces are dominant effects along with the curvature.

Experiments are performed for the B-type blade (see TABLE 1) in the pressure range of 0.1~4 Torr. Also, comparison between the experimental data and the DSMC results are presented in Figs. 9-11.

The pressure difference  $\Delta P (= P_2 - P_1)$  as a function of the throughput  $Q (= P_1 S$ , where  $S$  is the pumping speed) at  $P_1 = 0.076$  Torr is shown in Fig. 9. Comparison between the experimental data and the DSMC results shows good agreement.

The variations of pressure along the pumping passage at  $Q=0$  are shown in Fig. 10. In this figure, the measuring position 1, 2, 3, and 4 on the  $x$ -axis correspond to the location ①, ②, ③, and ④ in Fig. 4, respectively. As the outlet pressure  $P_2$  becomes lower,  $P_1$  decreases. In this figure, the dotted lines represent the DSMC results at  $P_2 = 0.1, 0.3,$  and  $0.6$  Torr, respectively. It is seen that the DSMC results agree well with the experimental data.

The compression ratio  $K (= P_2 / P_1)$  increases as  $P_2$  decreases, as shown in Fig. 11. Also, the DSMC results for  $P_2 = 0.1, 0.3,$  and  $0.6$  Torr agree well with the experimental data.

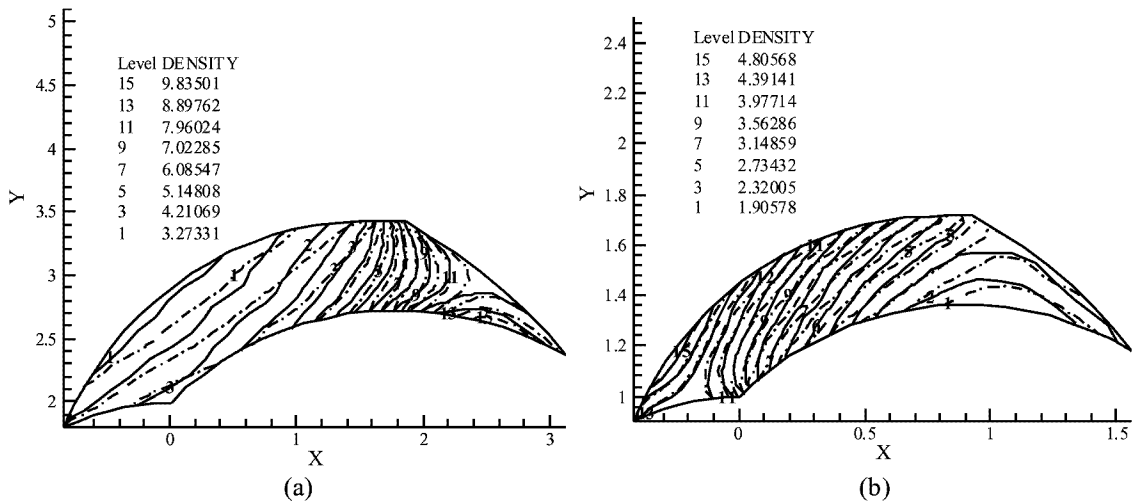


FIGURE 8. Density contours at  $P_1=0.076$  Torr and  $P_2=0.152$  Torr: (a) Type-II (+rps); (b) Type-II (-rps).

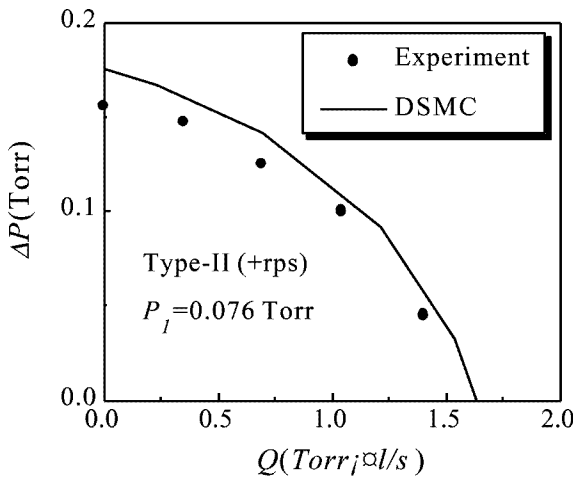


FIGURE 9. Performance curves.

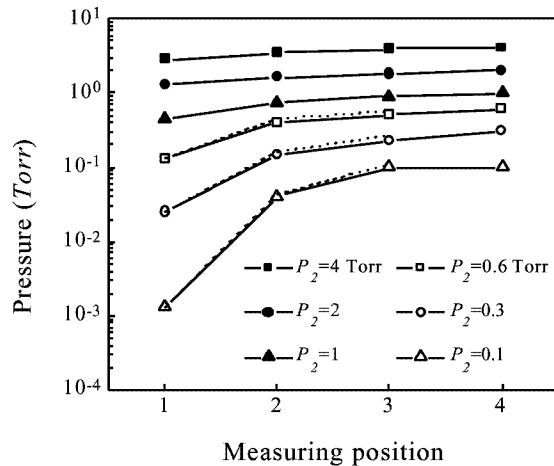
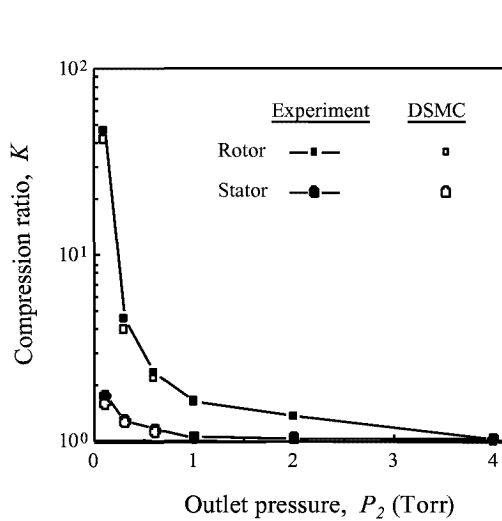
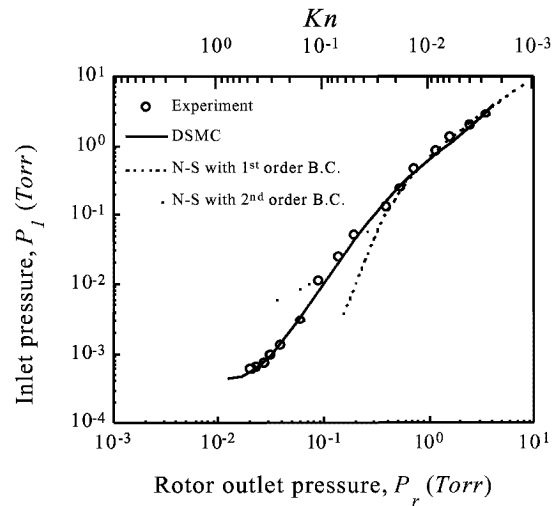


FIGURE 10. Pressure distribution along the channel.



**FIGURE 11.** Compression ratio vs. outlet pressure.



**FIGURE 12.** Effect of rotor outlet pressure on inlet pressure.

The effect of the rotor outlet pressure  $P_r$  on  $P_1$  at  $Q=0$  is shown in Fig. 12. In order to investigate the applicability of the N-S equations to the analysis of the molecular transition flow, the first- and second-order SBC, Eqs. (2) and (3), are included in the current N-S calculations. Comparison between the experimental data and the N-S results with first-order SBC shows good agreement in the range of the rotor outlet pressure  $P_r \geq 0.4$  Torr. But the significant discrepancy between the two results is seen in the range of  $P_r < 0.4$  Torr, *i.e.*,  $Kn > 0.02$ .

Consideration is now given to the effect of SBC on the N-S results. It is seen that the results obtained by the N-S method with second-order SBC are nearly the same as those with first-order SBC in the range of  $P_r \geq 0.4$  Torr and that the differences between the two results appear noticeably for  $P_r < 0.4$  Torr. Although the N-S method with second-order SBC fails to predict quantitatively the experimental data, it seems that the results obtained by second-order SBC agree reasonably in a qualitative way with the experimental data compared to those obtained by first-order SBC.

In general, for higher density flows, since the DSMC method cease to be computationally viable, the N-S method is usually much more efficient than the DSMC method. Thus, in the present analysis of flows which involve both molecular and slip flow regimes, it is reasonable to apply both methods. From Fig. 12, it is apparent that the slip flow analysis of the N-S method is inappropriate for  $Kn \geq 0.02$ , regardless of boundary conditions. Even so, Figure 12 shows a smooth transition in the flow description between the molecular and slip flow regimes. In addition, the N-S method simplifies the simulation and saves computational effort in predicting the performance in the slip flow regime. The present calculations have been performed by using double precision on a Silicon Graphics O2 (MIPS R10000 processor) workstation with 128Mbytes of memory. The computation time required for the N-S simulation is about 30 seconds. In contrast, the DSMC simulation takes approximately 48 hours of run time to obtain a converged solution.

Experimental results are also compared with those obtained by the DSMC simulations. The good agreement between the two is shown in Fig. 12. This clearly reveals the ability of the DSMC method to predict the molecular transition flows.

Finally, the variations of  $P_1$  as a function of  $P_r$  are illustrated in Fig. 13 for several volume flow rates. For a fixed volume flow rate, the DSMC method seems to be inappropriate, since such a fixed boundary condition can not be applied. So we calculate these curves by the N-S method with second-order SBC. The  $P_1$  becomes higher as the volume flow rate increases, and it depends on  $P_r$ . Comparison between the experimental data and the N-S results shows good agreement in the range of  $P_r \geq 0.4$  Torr. However, the apparent deviation of the N-S results from the experimental data can be seen for  $P_r < 0.4$  Torr.

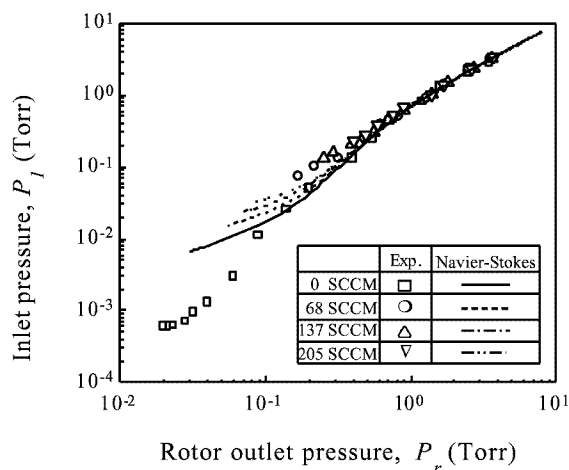


**FIGURE 13.** Effect of rotor outlet pressure on inlet pressure at several volume flow rates.

## CONCLUSIONS

Pumping performance of a DTDP has been numerically and experimentally analyzed. In the numerical study, the DSMC and N-S methods are employed to solve the problem of internal rarefied flows in pumping channels. The present experimental results in the pressure range of 0.1~4 Torr are compared with numerical ones obtained by both DSMC and N-S methods. The present results obtained by both numerical methods agree well with the experimental data for  $Kn \leq 0.02$ . In particular, it is found that the results obtained by second-order SBC agree qualitatively with the experimental data compared to those obtained by first-order SBC. Velocity and density fields were obtained by the DSMC simulations. Velocity components of the Type-II channel are much larger than those of the Type-I channel because the rotating disk imparts angular momentum directly to the molecules. Density contours show a large gradient near the outlet of channels.

## ACKNOWLEDGMENT

This work was supported by the Brain Korea 21 Project.

## REFERENCES

- Hablanian, M. H., in *Vacuum Science and Technology: Pioneers of 20th Century*, AIP, New York, 1994.
- Liu, N. and Pang, S. J., "Microscopic Theory of Drag Molecular Dynamics in the Range of Free Molecular Flow," *Vacuum*, Vol. 41, No. 7-9, 1990, pp. 2015-2017.
- Shi, L., Wang, X. Z., Zhu, Y. and Pang, S. J., "Design of Disk Molecular Pumps for Hybrid Molecular Pumps," *J. Vac. Sci. Technol. A*, Vol. 11, No. 2, 1993, pp. 426-431.
- Shi, L., Zhu, Y., Wang, X. Z. and Pang, S. J., "Influence of Clearance on the Pumping Performance of a Molecular Drag Pump," *J. Vac. Sci. Technol. A*, Vol. 11, No. 3, 1993, pp. 704-710.
- Cheng, H. P., Jou, R. Y., Chen, F. Z., Chang, Y. W., Iwane, M. and Hanaoka, T., "Flow Investigation of Siegbahn Vacuum Pump by CFD Methodology," *Vacuum*, Vol. 53, 1999, pp. 227-231.
- Heo, J. S. and Hwang, Y. K., "Molecular Transition and Slip Flows in the Pumping Channels of Drag Pumps," *J. Vac. Sci. Technol. A*, Vol. 18, No. 3, 2000, pp. 1025-1034.
- Bird, G. A., *Molecular Gas Dynamics and the Direct Simulation of Gas Flows*, Clarendon Press, Oxford, 1994.
- Koura, K., "Null-collision Technique in the Direct Simulation Monte Carlo Method," *Phys. Fluids*, Vol. 29, No. 11, 1986, pp. 3509-3511.
- Sawada, T., "Rarefied Gas Flow in a Rectangular Groove Facing a Moving Wall," *Sci. Papers of IPCR*, Vol. 70, No. 4, 1976, pp. 79-86.